Inorganic Chemistry

Article

pubs.acs.org/IC

Many Metals Make the Cut: Quaternary Rare-Earth Germanides $RE_4M_2InGe_4$ (M = Fe, Co, Ni, Ru, Rh, Ir) and $RE_4RhInGe_4$ Derived from Excision of Slabs in RE_2InGe_2

Anton O. Oliynyk, Stanislav S. Stoyko, and Arthur Mar*

Department of Chemistry, University of Alberta, Edmonton, Alberta, Canada T6G 2G2

Supporting Information

ABSTRACT: The formation of quaternary rare-earth (RE) germanides containing transition metals (M's) from groups 6 to 10 was investigated through arc-melting and annealing reactions at 800 °C; about 50 new compounds were obtained. These include several new series of quaternary germanides $RE_4M_2InGe_4$ (M = Fe, Co, Ru, Rh, Ir), previously known only for M = Mn and Ni; additional members of $RE_4Ni_2InGe_4$ extended to other RE substituents; and a different but closely related series $RE_4RhInGe_4$. Detailed crystal structures were determined by single-crystal X-ray diffraction studies for 20 compounds. Monoclinic structures in space group $C2/m$ are adopted by $RE_4M_2InGe_4$ ($Ho_4Ni_2InGe_4$-type, a = 15.1−16.5 Å, b = 4.1−4.4 Å, c = 6.9−7.3 Å, β = 106.2−108.6°) and $RE_4RhInGe_4$ (own type, a = 20.0−20.2 Å, b = 4.2−4.3 Å, c = 10.1−10.2 Å, β = 105.0−105.3°). Both structures contain frameworks built from MGe_4 tetrahedra, $InGe_4$ square planes, and Ge_2 dimers, delimiting tunnels occupied by RE atoms. These structures can also be derived by cutting slabs along different directions from the more symmetrical RE_2InGe_2 structure. Although the Ge_2 dimers are relatively invariant, the $InGe_4$ square planes can undergo distortion to form two sets of short versus long In−Ge distances. This distortion results from a competition between M−Ge bonding in the MGe_4 tetrahedra and In−Ge bonding in the $InGe_4$ square planes.

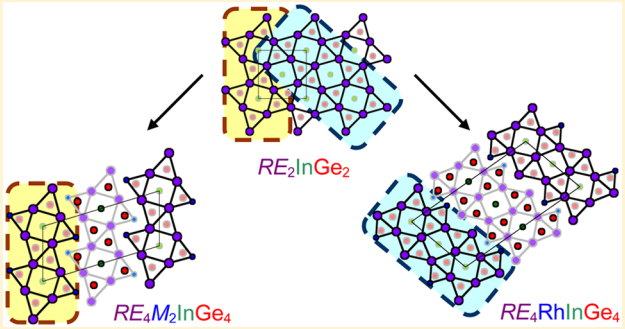

INTRODUCTION

Ternary rare-earth (RE) germanides RE−M−Ge are known for a wide variety of metal or metalloid components M, encompassing representatives from the s-block (Li, Mg), d-block (mostly first-row transition-metals from Mn to Cu, as well as some precious metals Ru−Ag and Os−Au), and p-block (Al, Ga, In, Si)[1] of the periodic table. These intermetallic compounds are of interest for their rich structural chemistry and diverse physical properties, including complex magnetic ordering (e.g., $RECrGe_3$),[2] magnetocaloric effects (e.g., $Gd_5(Si_xGe_{1-x})_4$),[3] and superconductivity (e.g., $RE_2Pt_3Ge_5$).[4] Among the examples containing a p-block metalloid, the RE_2InGe_2 phases are prevalent, forming for many RE components.[5−8] They adopt the tetragonal Mo_2FeB_2-type structure (an ordered variant of the U_3Si_2-type),[9] which exhibits some unusual features, the most remarkable of which are four-coordinate In atoms in rare square-planar geometry and Ge_2 dimers with strong bonds that are little affected by RE substitution. Some of the RE members can be prepared by stoichiometric reactions of the elements at high temperatures,[6,7] whereas others appear to require use of excess In acting as a flux.[8] Indeed, among the few known quaternary rare-earth germanides containing In, namely, $RE_4Ni_2InGe_4$ (RE = Dy, Ho, Er, Tm),[10] $RE_7Co_4InGe_{12}$ (RE = Dy, Ho, Yb),[11] and $Yb_3AuIn_3Ge_2$,[12] most were obtained, apparently serendipitously, from In flux reactions. It is unclear whether use of a flux is essential for the formation of these compounds, given that $RE_4Mn_2InGe_4$ (RE = La−Nd, Sm, Gd−Tm, Lu), reported recently by us,[13] and $RE_7Ni_{5-x}In_6Ge_{3+x}$ (RE = La−Nd, Sm) can be obtained by conventional methods.[14,15]

There is a close structural relationship between RE_2InGe_2 and $RE_4M_2InGe_4$ (M = Mn, Ni): the substitution within one of the RE sites by a transition-metal atom M in the structure of RE_2InGe_2, along with removal of some of the In atoms, leads to a cleavage of the three-dimensional framework into two-dimensional slabs found in the structure of $RE_4M_2InGe_4$. In this study, we investigate three hypotheses. First, we assert that all quaternary germanides $RE_4M_2InGe_4$ are thermodynamically stable phases that can be prepared through direct reactions of the elements. Second, we predict that new series of germanides $RE_4M_2InGe_4$ can be extended to many other transition-metal components M besides Mn and Ni. Third, we propose that new structures of quaternary germanides can be derived from cutting the framework of RE_2InGe_2 in different ways. After systematic synthetic experiments and structure determinations are carried out, we seek to understand the bonding interactions in these series with the aid of electronic band structure calculations.

Received: December 10, 2014
Published: March 2, 2015

DOI: 10.1021/ic502955h
Inorg. Chem. 2015, 54, 2780−2792

Table 1. Formation of Quaternary Germanides $RE_4M_2InGe_4$[a]

compound	La	Ce	Pr	Nd	Sm	Gd	Tb	Dy	Ho	Er	Tm	Lu
$RE_4Cr_2InGe_4$	–			–			–		–			
$RE_4Mo_2InGe_4$	–			–			–		–			
$RE_4W_2InGe_4$	–			–			–		–			
$RE_4Mn_2InGe_4$	+	+	+	+	+	+	+	+	+	+	+	+
$RE_4Re_2InGe_4$	–			–			–		–			
$RE_4Fe_2InGe_4$	–	+	+	+	+	+	+	+	+	+	+	+
$RE_4Ru_2InGe_4$	–	+	+	+	+	+	+	+	+	+	+	+
$RE_4Os_2InGe_4$	–			–			–		–			
$RE_4Co_2InGe_4$	–	+	+	+	+	+	+	+	+	+	+	+
$RE_4Rh_2InGe_4$	–	+	+	+	+	+	*	*	*	*	–	–
$RE_4Ir_2InGe_4$	+	+	+	+	–	–	–		–			
$RE_4Ni_2InGe_4$	–	–	–	–	+	+	+	+	+	+	+	–
$RE_4Pd_2InGe_4$					–	–	–	–	–	–	–	–
$RE_4Pt_2InGe_4$				–			–		–			

[a]Legend: known (+), unknown (−), alternative phase RE_4MInGe_4 forms (*), reaction not performed (blank entries), single-crystal structures determined (shaded in yellow). Except for $RE_4Mn_2InGe_4$ (all members)[13] and $RE_4Ni_2InGe_4$ (RE = Dy−Tm),[10] all results presented are from this work.

EXPERIMENTAL SECTION

Synthesis. Starting materials were freshly filed pieces of all the normally trivalent rare-earth metals (RE = La−Nd, Sm, Gd−Tm, Lu; 99.9%, Hefa), powders of various transition metals from groups 6 to 10 (M = Cr, Mo, W; Mn, Re; Fe, Ru, Os; Co, Rh, Ir; Ni, Pd, Pt; all greater than 99.9% purity, from Alfa-Aesar, Cerac, Spex, or Terochem), In shot (99.999%, Cerac), and Ge pieces (99.9999%, Alfa-Aesar). Mixtures of the elements with the nominal composition $RE_4M_2InGe_4$ were prepared with a total mass of 0.30 g for samples containing the cheaper transition metals or 0.20 g for those containing the precious metals. In initial experiments, only a few representative RE members (RE = La, Nd, Tb, Ho) were selected, and if the syntheses were successful for a given series, they were extended to other RE members. The samples were cold-pressed into pellets and arc-melted twice in a Centorr 5TA tri-arc furnace or an Edmund Bühler MAM-1 arc-melter on a water-cooled copper hearth under an argon atmosphere. Weight losses after arc-melting were less than 1%. The ingots were sealed in evacuated fused-silica tubes and annealed at 800 °C for one week, after which they were quenched in cold water. The products were ground and analyzed by powder X-ray diffraction (XRD), carried out with Cu $K\alpha_1$ radiation on an Inel diffractometer equipped with a curved position-sensitive detector (CPS 120). Table 1 summarizes the results of the reactions, indicating whether or not the synthesis of a given $RE_4M_2InGe_4$ member was successful. In the course of these reactions, a different Rh-containing series $RE_4RhInGe_4$ was found for some later RE members. Cell parameters for the quaternary phases were refined with use of the CSD suite of programs[16] and are listed in Table 2. Chemical compositions of selected crystals were determined by energy-dispersive X-ray (EDX) analysis on a JEOL JSM-6010LA InTouchScope scanning electron microscope, operated with an accelerating voltage of 20 kV and acquisition times of 70 s. All samples had compositions within 2% of values expected from the chemical formulas.

Although the synthetic investigations focused on trivalent RE components, the preparation of $Eu_4Fe_2InGe_4$ and $Yb_4Fe_2InGe_4$, which contain divalent RE components, was also attempted. Because Eu and Yb are too volatile to be arc-melted directly, a different procedure was used. Mixtures of elements in these nominal compositions were sealed within Ta tubes under an inert atmosphere of argon and heated at 800 °C for one week. Afterward, the sample was finely ground, pressed into pellets (with a mass loss of <2%), and arc-melted in a similar way as before. The resulting ingot was annealed at 800 °C for another week. The quaternary germanides were not formed, as shown by a representative powder XRD pattern for the $Yb_4Fe_2InGe_4$ reaction (Figure S1 in Supporting Information).

Structure Determination. Suitable single crystals, which were gray and irregularly shaped, were found for many members of the $RE_4M_2InGe_4$ (M = Fe, Co, Ru, Rh) series. Intensity data were collected on a Bruker PLATFORM diffractometer equipped with a SMART APEX II CCD detector and a graphite-monochromated Mo $K\alpha$ radiation source, using ω scans at 6−8 different ϕ angles with a frame width of 0.3° and an exposure time of 12−30 s per frame. Face-indexed numerical absorption corrections were applied. Structure solution and refinement were carried out with use of the SHELXTL (version 6.12) program package.[17] The Laue symmetry, systematic absences, and intensity statistics established the centrosymmetric monoclinic space group $C2/m$; direct methods suggested models consistent with the $Ho_4Ni_2InGe_4$-type structure. Atomic coordinates were standardized with use of the program STRUCTURE TIDY.[18] There have been previous reports of a small In substoichiometry observed in structural refinements of related compounds.[10,13] In a separate investigation of the phase equilibria in the Ce−Mn−In−Ge system, metallographic and XRD analyses confirm that $Ce_4Mn_2InGe_4$ exhibits an In substoichiometry that is indeed intrinsic and fixed (~93%), with no homogeneity range.[19] Thus, the occupancies of all sites were successively freed in later stages of refinement. The occupancy of the In site ranged from 0.93(2) to 0.99(2), whereas the occupancies for all other sites did not deviate significantly from unity, 1.00(2). In most cases, the occupancy of the In site is quite close to unity, and it is difficult to judge whether the slight substoichiometry is physically meaningful or an artifact (e.g., from inadequate absorption correction). The displacement parameters for the In site are always slightly greater than those of the other atoms, but this feature probably reflects the unusually low coordination of this site. Nevertheless, to

DOI: 10.1021/ic502955h
Inorg. Chem. 2015, 54, 2780−2792

Table 2. Cell Parameters (from Powder Diffraction Data) for $RE_4M_2InGe_4$ (M = Fe, Co, Ru, Rh, Ir) and $RE_4RhInGe_4$

compound	a (Å)	b (Å)	c (Å)	β (deg)	V (Å^3)
$RE_4Fe_2InGe_4$					
$Ce_4Fe_2InGe_4$	16.078(1)	4.376(1)	7.305(1)	107.151(8)	491.2(2)
$Pr_4Fe_2InGe_4$	16.0469(6)	4.3386(6)	7.2495(4)	106.954(7)	482.8(1)
$Nd_4Fe_2InGe_4$	15.967(2)	4.3176(8)	7.2351(8)	107.17(1)	476.6(2)
$Sm_4Fe_2InGe_4$	15.781(1)	4.2725(7)	7.1240(6)	107.050(8)	459.2(2)
$Gd_4Fe_2InGe_4$	15.706(2)	4.250(2)	7.081(4)	106.97(3)	452.1(4)
$Tb_4Fe_2InGe_4$	15.623(1)	4.2311(8)	7.0412(5)	107.129(8)	444.8(2)
$Dy_4Fe_2InGe_4$	15.538(2)	4.2125(6)	6.9956(9)	106.976(8)	437.9(2)
$Ho_4Fe_2InGe_4$	15.519(2)	4.200(1)	6.9785(6)	107.13(1)	434.7(2)
$Er_4Fe_2InGe_4$	15.449(2)	4.1783(9)	6.945(1)	107.02(1)	428.7(2)
$Tm_4Fe_2InGe_4$	15.406(2)	4.1734(6)	6.9220(8)	107.146(8)	425.3(2)
$Lu_4Fe_2InGe_4$	15.342(3)	4.150(1)	6.8868(7)	107.233(6)	418.8(2)
$RE_4Co_2InGe_4$					
$Ce_4Co_2InGe_4$	15.990(1)	4.3504(6)	7.288(1)	107.66(1)	483.1(2)
$Pr_4Co_2InGe_4$	15.847(4)	4.3415(9)	7.2376(8)	107.425(8)	475.1(3)
$Nd_4Co_2InGe_4$	15.8443(6)	4.3167(4)	7.2065(4)	107.603(8)	469.8(1)
$Sm_4Co_2InGe_4$	15.692(1)	4.2823(7)	7.1341(7)	107.714(5)	456.7(2)
$Gd_4Co_2InGe_4$	15.563(2)	4.241(1)	7.061(1)	107.74(1)	443.9(2)
$Tb_4Co_2InGe_4$	15.4676(7)	4.2350(9)	7.0240(5)	107.66(2)	438.4(2)
$Dy_4Co_2InGe_4$	15.406(3)	4.213(1)	6.9904(4)	107.653(9)	432.4(2)
$Ho_4Co_2InGe_4$	15.364(2)	4.1979(7)	6.9698(4)	107.663(5)	428.3(2)
$Er_4Co_2InGe_4$	15.321(2)	4.1834(6)	6.9491(4)	107.67(1)	424.4(2)
$Tm_4Co_2InGe_4$	15.256(2)	4.181(1)	6.9215(7)	107.694(7)	420.6(2)
$Lu_4Co_2InGe_4$	15.193(1)	4.154(1)	6.8851(8)	107.712(7)	413.9(2)
$RE_4Ni_2InGe_4$					
$Sm_4Ni_2InGe_4$	15.685(3)	4.281(1)	7.133(1)	107.68(2)	456.3(3)
$Gd_4Ni_2InGe_4$	15.532(1)	4.2662(8)	7.111(2)	107.73(1)	448.8(3)
$Tb_4Ni_2InGe_4$	15.4471(9)	4.232(1)	7.069(1)	107.75(3)	440.1(3)
$Dy_4Ni_2InGe_4$	15.410(1)	4.2177(9)	7.0170(4)	108.62(1)	432.2(2)
$Ho_4Ni_2InGe_4$	15.388(2)	4.2074(9)	6.9976(9)	108.542(4)	429.5(2)
$Er_4Ni_2InGe_4$	15.346(1)	4.1936(7)	6.9786(5)	108.511(8)	425.9(1)
$Tm_4Ni_2InGe_4$	15.316(3)	4.1730(9)	6.9618(9)	108.51(1)	421.9(3)
$RE_4Ru_2InGe_4$					
$Ce_4Ru_2InGe_4$	16.194(1)	4.3821(9)	7.2449(3)	106.239(9)	493.6(2)
$Pr_4Ru_2InGe_4$	16.1110(9)	4.3678(7)	7.2024(4)	106.286(8)	486.5(2)
$Nd_4Ru_2InGe_4$	16.029(2)	4.351(1)	7.1691(4)	106.366(9)	479.7(2)
$Sm_4Ru_2InGe_4$	15.900(1)	4.3175(4)	7.1022(4)	106.546(5)	467.4(1)
$Gd_4Ru_2InGe_4$	15.794(1)	4.291(1)	7.0447(5)	106.608(7)	457.5(2)
$Tb_4Ru_2InGe_4$	15.676(1)	4.2681(9)	6.9902(5)	106.666(5)	448.0(2)
$Dy_4Ru_2InGe_4$	15.638(1)	4.2600(8)	6.9732(5)	106.765(9)	444.8(2)
$Ho_4Ru_2InGe_4$	15.581(1)	4.2385(7)	6.9472(4)	106.766(5)	439.3(1)
$Er_4Ru_2InGe_4$	15.552(2)	4.2286(7)	6.9205(5)	106.843(6)	435.6(2)
$Tm_4Ru_2InGe_4$	15.492(1)	4.2257(8)	6.9053(6)	106.890(8)	432.6(2)
$Lu_4Ru_2InGe_4$	15.458(1)	4.2033(7)	6.8721(4)	107.01(1)	427.0(1)
$RE_4Rh_2InGe_4$					
$Ce_4Rh_2InGe_4$	16.192(1)	4.3897(7)	7.2480(6)	106.829(7)	493.1(2)
$Pr_4Rh_2InGe_4$	16.146(1)	4.378(1)	7.2236(5)	106.856(9)	488.7(2)
$Nd_4Rh_2InGe_4$	16.0389(8)	4.3549(9)	7.1800(6)	106.91(1)	479.8(2)
$Sm_4Rh_2InGe_4$	15.910(1)	4.3226(8)	7.1131(3)	107.000(8)	467.8(2)
$Gd_4Rh_2InGe_4$	15.793(2)	4.3167(8)	7.0665(4)	107.10(1)	460.5(2)
$RE_4Ir_2InGe_4$					
$La_4Ir_2InGe_4$	16.548(2)	4.4152(8)	7.3445(6)	106.798(8)	513.7(2)
$Ce_4Ir_2InGe_4$	16.269(2)	4.3643(7)	7.2217(8)	106.953(8)	490.5(2)
$Pr_4Ir_2InGe_4$	16.166(1)	4.3464(6)	7.195(2)	106.92(2)	483.7(3)
$Nd_4Ir_2InGe_4$	16.156(2)	4.3428(6)	7.1839(7)	107.034(8)	481.9(2)
$RE_4RhInGe_4$					
$Tb_4RhInGe_4$	20.221(3)	4.251(1)	10.227(2)	105.01(2)	849.1(6)
$Dy_4RhInGe_4$	20.181(2)	4.238(2)	10.225(1)	105.11(1)	844.3(6)
$Ho_4RhInGe_4$	20.110(2)	4.2162(7)	10.220(1)	105.21(1)	836.2(3)
$Er_4RhInGe_4$	20.029(2)	4.2109(9)	10.161(1)	105.29(1)	826.6(4)

DOI: 10.1021/ic502955h
Inorg. Chem. 2015, 54, 2780−2792

Table 3. Crystallographic Data for $RE_4M_2InGe_4$ (M = Fe, Co, Ru, Rh) and $Tb_4RhInGe_4$[a]

formula	fw (amu)	a (Å)	b (Å)	c (Å)	β (deg)	V (Å^3)	ρ_c (g cm^{-3})	μ (mm^{-1})	$R(F)$[b]	$R_w(F_0^2)$[c]
$Ce_4Fe_2In_{0.969(2)}Ge_4$	1077.36	16.071(4)	4.3480(10)	7.2757(17)	106.945(3)	486.34(19)	7.357	35.58	0.017	0.039
$Pr_4Fe_2In_{0.974(3)}Ge_4$	1080.52	16.0089(12)	4.3242(3)	7.2282(5)	106.8770(10)	478.83(6)	7.494	37.48	0.020	0.039
$Nd_4Fe_2In_{0.987(2)}Ge_4$	1093.84	15.9354(10)	4.3102(3)	7.2004(5)	107.0650(9)	472.78(6)	7.684	39.31	0.017	0.037
$Sm_4Fe_2In_{0.964(3)}Ge_4$	1118.28	15.770(4)	4.2745(11)	7.1211(17)	107.011(3)	459.0(2)	8.091	43.45	0.020	0.041
$Gd_4Fe_2In_{0.983(5)}Ge_4$	1145.88	15.672(3)	4.2436(8)	7.0643(13)	107.068(3)	449.12(14)	8.473	47.80	0.031	0.069
$Ce_4Co_2In_{0.986(3)}Ge_4$	1083.52	15.9351(14)	4.3361(4)	7.2602(6)	107.5309(12)	478.35(7)	7.523	36.61	0.022	0.045
$Pr_4Co_2In_{0.985(2)}Ge_4$	1086.68	15.8705(6)	4.3247(2)	7.2264(3)	107.5111(5)	473.00(3)	7.630	38.38	0.016	0.034
$Nd_4Co_2In_{0.965(2)}Ge_4$	1100.00	15.7845(9)	4.3028(3)	7.1824(4)	107.5115(8)	465.20(5)	7.853	40.40	0.018	0.037
$Sm_4Co_2In_{0.973(2)}Ge_4$	1124.44	15.6336(12)	4.2723(3)	7.1131(6)	107.6415(10)	452.75(6)	8.248	44.52	0.016	0.033
$Gd_4Co_2In_{0.970(4)}Ge_4$	1152.04	15.548(6)	4.2483(16)	7.058(3)	107.618(5)	444.3(5)	8.610	48.78	0.026	0.054
$Ce_4Ru_2In_{0.962(3)}Ge_4$	1167.80	16.174(4)	4.3794(10)	7.2321(17)	106.144(3)	492.1(2)	7.882	35.29	0.022	0.051
$Pr_4Ru_2In_{0.959(5)}Ge_4$	1170.96	16.083(5)	4.3605(13)	7.190(2)	106.254(4)	484.1(2)	8.033	37.20	0.035	0.081
$Nd_4Ru_2In_{0.954(3)}Ge_4$	1184.28	16.014(6)	4.3463(16)	7.160(3)	106.353(5)	478.2(3)	8.225	38.99	0.024	0.053
$Sm_4Ru_2In_{0.965(3)}Ge_4$	1208.72	15.877(3)	4.3178(7)	7.0936(12)	106.517(2)	466.23(13)	8.610	42.91	0.022	0.044
$Gd_4Ru_2In_{0.962(3)}Ge_4$	1236.32	15.773(4)	4.2875(11)	7.0393(18)	106.635(4)	456.1(2)	9.002	47.20	0.024	0.044
$Tb_4Ru_2In_{0.932(3)}Ge_4$	1243.00	15.6651(9)	4.2639(2)	6.9895(4)	106.672(1)	447.23(4)	9.230	50.10	0.019	0.043
$Dy_4Ru_2In_{0.961(4)}Ge_4$	1257.32	15.612(3)	4.2519(9)	6.9641(15)	106.728(3)	442.73(16)	9.432	52.42	0.024	0.051
$Ho_4Ru_2In_{0.962(4)}Ge_4$	1267.04	15.550(4)	4.2349(12)	6.9425(19)	106.842(4)	437.6(2)	9.617	55.05	0.023	0.054
$Er_4Ru_2In_{0.980(5)}Ge_4$	1276.36	15.526(5)	4.2254(14)	6.916(2)	106.850(4)	434.2(2)	9.762	57.68	0.030	0.069
$Sm_4Rh_2In_{0.973(3)}Ge_4$	1212.40	15.857(3)	4.3147(8)	7.0971(14)	106.878(3)	464.65(16)	8.666	43.36	0.020	0.039
$Tb_4RhInGe_4$	1143.77	20.2575(12)	4.2641(3)	10.2434(6)	104.9984(9)	854.68(9)	8.889	50.89	0.024	0.058

[a]For all structures, λ = 0.710 73 Å, space group $C2/m$ (No. 12). For $RE_4M_2InGe_4$ (M = Fe, Co, Ru, Rh), T = 173(2) K and Z = 2; for $Tb_4RhInGe_4$, T = 296(2) K and Z = 4. [b]$R(F) = \sum||F_o| - |F_c||/\sum|F_o|$ for $F_o^2 > 2\sigma(F_o^2)$. [c]$R_w(F_o^2) = [\sum[w(F_o^2 - F_c^2)^2]/\sum wF_o^4]^{1/2}$; $w^{-1} = [\sigma^2(F_o^2) + (Ap)^2 + Bp]$, where $p = [\max(F_o^2,0) + 2F_c^2]/3$.

ensure consistency among all structure determinations, the In occupancy was treated as a variable parameter.

Within the different $RE_4RhInGe_4$ series, a suitable crystal could be found for the Tb member for data collection. $Tb_4RhInGe_4$ also crystallizes in the monoclinic space group $C2/m$; its cell parameters a and c are different from those in $RE_4M_2InGe_4$, but b is similar (~4 Å), suggesting that their structures are related. Direct methods revealed locations of all atoms and refinements proceeded in a straightforward manner. Here there was no evidence of an In substoichiometry, and the ideal formula $Tb_4RhInGe_4$ was retained.

Table 3 lists abbreviated crystal data and experimental details, and Table 4 lists ranges of interatomic distances. Full crystallographic data for all structures, including all atomic coordinates and individual interatomic distances, are provided in Tables S1–S12 as Supporting Information. Further data in the form of crystallographic information files (CIFs) are available as Supporting Information.

Band Structure Calculations. Tight-binding linear muffin tin orbital (LMTO) band structure calculations were performed within the local density and atomic spheres approximation with use of the Stuttgart TB-LMTO-ASA program (version 4.7).[20] To avoid computational difficulties associated with 4f orbitals of RE atoms, the model compounds $La_4M_2InGe_4$ (M = Mn, Fe, Co, Ru) and $Y_4RhInGe_4$ containing nonmagnetic RE components were considered. Cell parameters and atomic positions for $La_4M_2InGe_4$ were taken from the corresponding Ce members because the La members are unknown except for the Mn-containing series; similarly, structural parameters for $Y_4RhInGe_4$ were taken from those of the crystallographically characterized Tb member. For $La_4M_2InGe_4$, the basis sets consisted of La 6s/6p/5d/4f, M 4s/4p/3d (for Mn, Fe, Co) or 5s/5p/4d/4f (for Ru), In 5s/5p/5d/4f, and Ge 4s/4p/4d orbitals, with the La 6p/4f, In 5d/4f, and Ge 4d orbitals being downfolded; for $Y_4RhInGe_4$, the basis set consisted of Y 5s/5p/4d/4f, Rh 5s/5p/4d/4f, In 5s/5p/5d/4f, and Ge 4s/4p/4d orbitals, with the Y 5p/4f, Rh 4f, In 5d/4f, and Ge 4d orbitals being downfolded. Integrations in reciprocal space were performed with an improved tetrahedron method over 554 irreducible k points (from a 16 × 16 × 8 mesh) within the first Brillouin zone. To understand the effect of distortion on the $InGe_4$ square plane, hypothetical structures were examined for $La_4Fe_2InGe_4$ in which the atomic coordinates of Ge1 and Ge2 were adjusted such that the In–Ge1 distances contract, while the In–Ge2 distances expand in increments (Δx) of 0.05 Å from an idealized square plane with equal In–Ge distances, while the bond angles around the In atom were fixed (close to 90°).

Magnetic Susceptibility Measurement. The Sm-containing samples, $Sm_4M_2InGe_4$ (M = Fe, Co, Ru, Rh) were found to be free of impurity phases and were suitable for magnetic susceptibility measurements. The direct current magnetic susceptibility was measured under an applied field of 0.5 T between 2 and 300 K on a Quantum Design 9T-PPMS magnetometer. Susceptibility values were corrected for contributions from the holder and sample diamagnetism.

RESULTS AND DISCUSSION

To investigate the formation of quaternary germanides $RE_4M_2InGe_4$, a total of 115 samples were prepared by arc-melting mixtures of the elements followed by annealing at 800 °C for one week. Given that the previously known series were limited to M = Mn and Ni,[10,13] attempts were made to substitute all other transition-metal elements from groups 6 to 10 (except Tc). For a fixed M, the RE components were initially restricted to La, Nd, Tb, and Ho, and then extended to other trivalent RE metals if the syntheses were successful. The existence of $RE_4M_2InGe_4$ phases was confirmed for a wide variety of metals from groups 7 (Mn), 8 (Fe, Ru), 9 (Co, Rh, Ir), and 10 (Ni) (Table 1). The quaternary germanides $RE_4M_2InGe_4$ constituted the major phase in the products; the most common minor phases present were typically ternary germanides RE_2InGe_2 and REM_2Ge_2, in varying amounts depending on the system. Analysis of the products and powder XRD patterns for the $Nd_4M_2InGe_4$ and $Sm_4M_2InGe_4$ reactions, chosen as representative examples, are provided in Table S13 and Figures S2 and S3 in Supporting Information. For $Sm_4M_2InGe_4$, the products are nearly phase-pure, whereas for $Nd_4M_2InGe_4$, further synthetic optimization is necessary to improve sample homogeneity, which would benefit from

DOI: 10.1021/ic502955h
Inorg. Chem. 2015, 54, 2780–2792

Table 4. Ranges of Interatomic Distances (Å) for $RE_4M_2InGe_4$ (M = Fe, Co, Ru, Rh) and $Tb_4RhInGe_4$

compound	RE−Ge	RE−M	RE−In	M−Ge	In−Ge	Ge−Ge
$Ce_4Fe_2In_{0.969(2)}Ge_4$	3.0543(6)−3.4490(8)	3.1351(11)−3.5205(8)	3.3951(6)−3.4591(6)	2.4612(6)−2.4996(10)	3.0088(8)−3.4185(9)	2.5834(10)
$Pr_4Fe_2In_{0.974(3)}Ge_4$	3.0311(5)−3.4545(7)	3.1244(9)−3.4933(7)	3.3810(3)−3.4413(3)	2.4529(5)−2.4944(10)	2.9854(6)−3.3887(7)	2.5803(12)
$Nd_4Fe_2In_{0.987(2)}Ge_4$	3.0108(4)−3.4511(6)	3.1068(7)−3.4749(6)	3.3742(3)−3.4349(3)	2.4524(4)−2.4980(9)	2.9726(5)−3.3412(6)	2.5701(10)
$Sm_4Fe_2In_{0.964(3)}Ge_4$	2.9742(7)−3.4470(9)	3.0692(11)−3.4409(9)	3.3404(6)−3.4048(6)	2.4392(7)−2.4924(12)	2.9333(8)−3.2790(9)	2.5615(13)
$Gd_4Fe_2In_{0.983(5)}Ge_4$	2.9445(9)−3.4429(14)	3.0479(18)−3.4076(13)	3.3257(6)−3.3849(6)	2.4312(11)−2.484(2)	2.9099(12)−3.2302(13)	2.547(2)
$Ce_4Co_2In_{0.986(3)}Ge_4$	3.0399(6)−3.3859(8)	3.0855(10)−3.5304(8)	3.3957(3)−3.4571(3)	2.4439(5)−2.4800(11)	3.0056(7)−3.3725(8)	2.5884(13)
$Pr_4Co_2In_{0.985(2)}Ge_4$	3.0258(4)−3.3858(5)	3.0701(6)−3.5153(5)	3.3822(2)−3.4499(2)	2.4405(3)−2.4790(7)	2.9870(5)−3.3425(6)	2.5810(9)
$Nd_4Co_2In_{0.965(2)}Ge_4$	3.0017(4)−3.3852(6)	3.0536(8)−3.4955(6)	3.3608(3)−3.4317(3)	2.4338(4)−2.4699(9)	2.9657(6)−3.3075(7)	2.5731(10)
$Sm_4Co_2In_{0.973(2)}Ge_4$	2.9680(4)−3.3785(6)	3.0168(7)−3.4674(5)	3.3360(2)−3.4075(3)	2.4262(4)−2.4656(8)	2.9335(5)−3.2372(6)	2.5570(9)
$Gd_4Co_2In_{0.970(4)}Ge_4$	2.9400(10)−3.3814(14)	2.9995(17)−3.4338(12)	3.3209(9)−3.3924(9)	2.4234(10)−2.4683(17)	2.9044(13)−3.1907(14)	2.5493(19)
$Ce_4Ru_2In_{0.962(3)}Ge_4$	3.0495(7)−3.4922(10)	3.1433(9)−3.5311(7)	3.3929(6)−3.4867(6)	2.4792(6)−2.5273(10)	2.9789(9)−3.4512(10)	2.6063(14)
$Pr_4Ru_2In_{0.959(5)}Ge_4$	3.0319(12)−3.4880(16)	3.1249(14)−3.5054(11)	3.3800(8)−3.4736(8)	2.4740(9)−2.5243(16)	2.9552(14)−3.4039(15)	2.594(2)
$Nd_4Ru_2In_{0.954(3)}Ge_4$	3.0178(9)−3.4890(13)	3.1141(13)−3.4863(10)	3.3686(9)−3.4614(9)	2.4728(9)−2.5184(13)	2.9401(12)−3.3660(13)	2.5796(17)
$Sm_4Ru_2In_{0.965(3)}Ge_4$	2.9849(6)−3.4890(9)	3.0846(8)−3.4472(6)	3.3533(5)−3.4389(5)	2.4685(5)−2.5112(9)	2.9051(8)−3.2896(9)	2.5609(15)
$Gd_4Ru_2In_{0.962(3)}Ge_4$	2.9536(8)−3.4947(12)	3.0685(11)−3.4113(8)	3.3370(7)−3.4123(7)	2.4626(7)−2.5078(13)	2.8757(10)−3.2324(11)	2.5463(18)
$Tb_4Ru_2In_{0.932(3)}Ge_4$	2.9289(4)−3.5055(6)	3.0494(6)−3.3829(4)	3.3192(2)−3.3874(2)	2.4582(4)−2.5100(8)	2.8429(6)−3.1781(7)	2.5380(12)
$Dy_4Ru_2In_{0.961(4)}Ge_4$	2.9182(8)−3.4955(9)	3.0343(9)−3.3687(7)	3.3138(6)−3.3828(6)	2.4545(7)−2.5107(13)	2.8341(10)−3.1540(11)	2.5284(18)
$Ho_4Ru_2In_{0.962(4)}Ge_4$	2.9011(8)−3.5013(11)	3.0263(11)−3.3514(8)	3.3044(7)−3.3654(7)	2.4520(8)−2.5123(13)	2.8187(10)−3.1202(11)	2.5245(17)
$Er_4Ru_2In_{0.980(5)}Ge_4$	2.8931(11)−3.5009(14)	3.0196(14)−3.3355(10)	3.3025(8)−3.3612(8)	2.4518(10)−2.5120(17)	2.8076(14)−3.1001(15)	2.513(3)
$Sm_4Rh_2In_{0.973(3)}Ge_4$	2.9777(6)−3.5543(9)	3.0788(8)−3.4434(6)	3.3891(5)−3.4219(5)	2.4964(5)−2.5342(9)	2.9013(8)−3.2141(8)	2.5569(13)
$Tb_4RhInGe_4$	2.9166(9)−3.4498(9)	3.0761(7)−3.3288(5)	3.3673(3)−3.4358(3)	2.4703(5)−2.5524(10)	2.8177(9)−3.0700(9)	2.5958(12)−2.6192(12)

DOI: 10.1021/ic502955h
Inorg. Chem. 2015, 54, 2780−2792

additional annealing treatments. Attempts were also made to prepare $Eu_4Fe_2InGe_4$ and $Yb_4Fe_2InGe_4$, which contain divalent RE members, by arc-melting pretreated sintered pellets of mixtures of the elements, but these were unsuccessful.

The extent of RE substitution varies depending on the identity of M. The Mn-containing series is the most extensive, forming for all lanthanides from La to Lu (except Eu and Yb, which are too volatile to be suitable for arc-melting reactions, and Pm, which is radioactive). The Fe-, Ru-, and Co-containing series are almost as extensive, except that the La members do not form. In the progression down the Co-triad metals, the extent of RE substitution gradually becomes narrower until only the largest members (La–Nd) are found for $RE_4Ir_2InGe_4$. An unexpected result of these synthetic experiments is that although $RE_4Rh_2InGe_4$ forms for RE = La–Nd, Sm, Gd, a different series $RE_4RhInGe_4$ was discovered for RE = Tb–Er. The Ni-containing series was previously known for RE = Dy–Tm; it was suggested that this series could only be prepared through use of an In flux but not through arc-melting or induction-melting reactions.[10] However, the present investigation indicates that not only can this series be formed through arc-melting and annealing, it can also be extended to include RE = Sm, Gd, and Tb. Conversely, we attempted to prepare $Sm_4Fe_2InGe_4$, which can be easily obtained phase-pure from stoichiometric reaction of the elements, in the presence of a 10-fold excess of In, using the identical heat treatment used in the flux synthesis of $RE_4Ni_2InGe_4$, followed by removal of molten In by centrifugation. Large crystals of the binary germanide Sm_5Ge_3 resulted from this In-flux reaction instead (Figure S4 in Supporting Information). Thus, it is not straightforward to extrapolate from these observations whether a given $RE_4M_2InGe_4$ member exists or not, if only an In-flux reaction is performed; in fact, as shown here, use of excess In may turn out to be detrimental if other competing phases crystallize preferentially.

Cell parameters determined from powder XRD data (Table 2) generally follow expected trends. Within any series of fixed M, the cell volume decreases in accordance with the lanthanide contraction (Figure 1). Among the series containing the 3d metals Mn, Fe, Co, and Ni, the cell volume curves shift downward, reflecting the trend in decreasing metallic radii of these elements on proceeding across the periodic table. The cell volume curves for $RE_4Ni_2InGe_4$ and $RE_4Co_2InGe_4$ are nearly coincident, suggesting that perhaps with appropriate changes in synthetic conditions, it may be possible to extend the Ni-containing series to further RE members. Among the series containing the 4d and 5d metals Ru, Rh, and Ir, the cell volume curves almost overlap; the trend in increasing metallic radii in this progression is reflected instead in the compatibility with larger RE components. These observations suggest that both size factors involving well-matched combinations of RE and M components and electronic factors restricting the M component to groups 7–10 are important in the stability of these compounds. If group 6 metals are excluded from consideration (given that none were found to form $RE_4M_2InGe_4$ phases in the synthetic experiments, presumably because the electron count is too low), then a structure map created by plotting the Pauling metallic radii[21] of RE and M is reasonably effective in delimiting the regions in which $RE_4M_2InGe_4$ forms (Figure 2). At the boundary defining the upper limit of the radius of M (near 1.25 Å), the alternative phase $RE_4RhInGe_4$ forms within only a very narrow region. Substitution of the M component in structurally related ternary rare-earth germanides such as

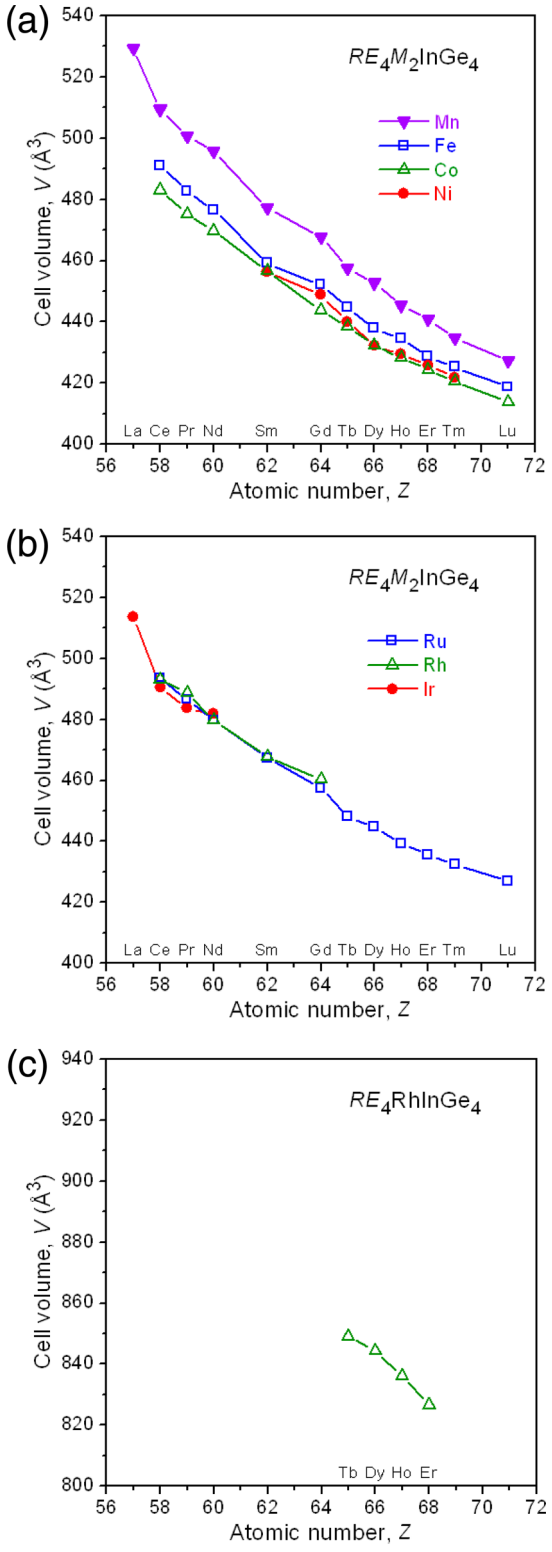

Figure 1. Plots of unit cell volumes for (a) $RE_4M_2InGe_4$ (M = Mn, Fe, Co, Ni), (b) $RE_4M_2InGe_4$ (M = Ru, Rh, Ir), and (c) $RE_4RhInGe_4$. Data for $RE_4Mn_2InGe_4$ are taken from ref 13.

RE_2MGe_2 (Sc_2CoSi_2-type) and REM_2Ge_2 ($CeAl_2Ga_2$-type) also appear to be restricted to later transition metals;[22] it would be interesting to develop a more generalized structure map applicable to a broader set of such phases.

To the best of our ability, we evaluated as many single crystals as possible for their suitability for further X-ray

DOI: 10.1021/ic502955h
Inorg. Chem. 2015, 54, 2780–2792

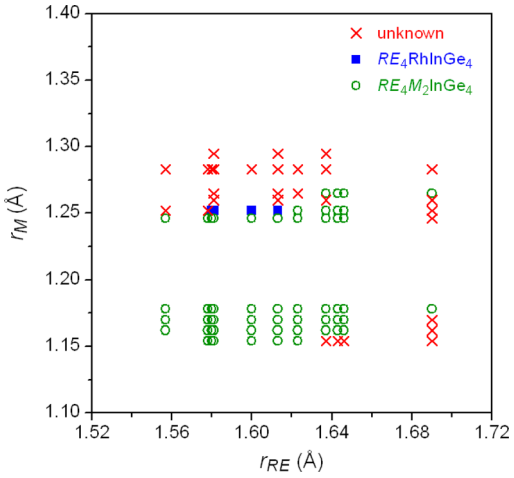

Figure 2. Structure map defined by Pauling metallic radii of RE and M components.

diffraction experiments. Within the four $RE_4M_2InGe_4$ series containing M = Fe, Co, Ni, and Ru, 20 structure determinations were performed; unfortunately, suitable crystals could not be found for any of the Ir-containing members. Within the new $RE_4RhInGe_4$ series, the crystal structure was determined solely for the Tb member. Both $RE_4M_2InGe_4$ ($Ho_4Ni_2InGe_4$-type) and $RE_4RhInGe_4$ (new type) adopt monoclinic structures with similar values of the short-axis parameter ($b \approx 4.3$ Å). In terms of a conventional description focused on the covalent framework, both structures contain the same building blocks of MGe_4 tetrahedra, $InGe_4$ square planes, and Ge_2 dimers (Figure 3). The MGe_4 tetrahedra are connected through edges and corners to form infinite double chains extending along the *b*-direction. (These double chains could also be described as ladders made of M−Ge rungs or ribbons made of M_2Ge_2 rhombi.) In $RE_4M_2InGe_4$, one of the four Ge atoms surrounding each tetrahedrally coordinated M atom belongs to a Ge_2 dimer, which acts to connect adjacent double chains along the *a*-direction to generate $[M_2Ge_4]$ layers parallel to the *ab*-plane. Indium atoms in square planar coordination then connect these layers together, delimiting two types of tunnels: a smaller pentagonal one filled by RE2 atoms and a larger oblique one (outlined by an eight-membered ring) filled by RE1 atoms. In $RE_4RhInGe_4$, all four Ge atoms surrounding each Rh atom belong to Ge_2 dimers, which are not connected directly to adjacent double chains but rather through the intermediary of the In atoms. Two types of pentagonal tunnels are separately filled by the RE2 and RE4 atoms, and a large irregularly shaped (12-membered ring) one is filled by the RE1 and RE3 atoms. The double chains of tetrahedra appear to be a common motif

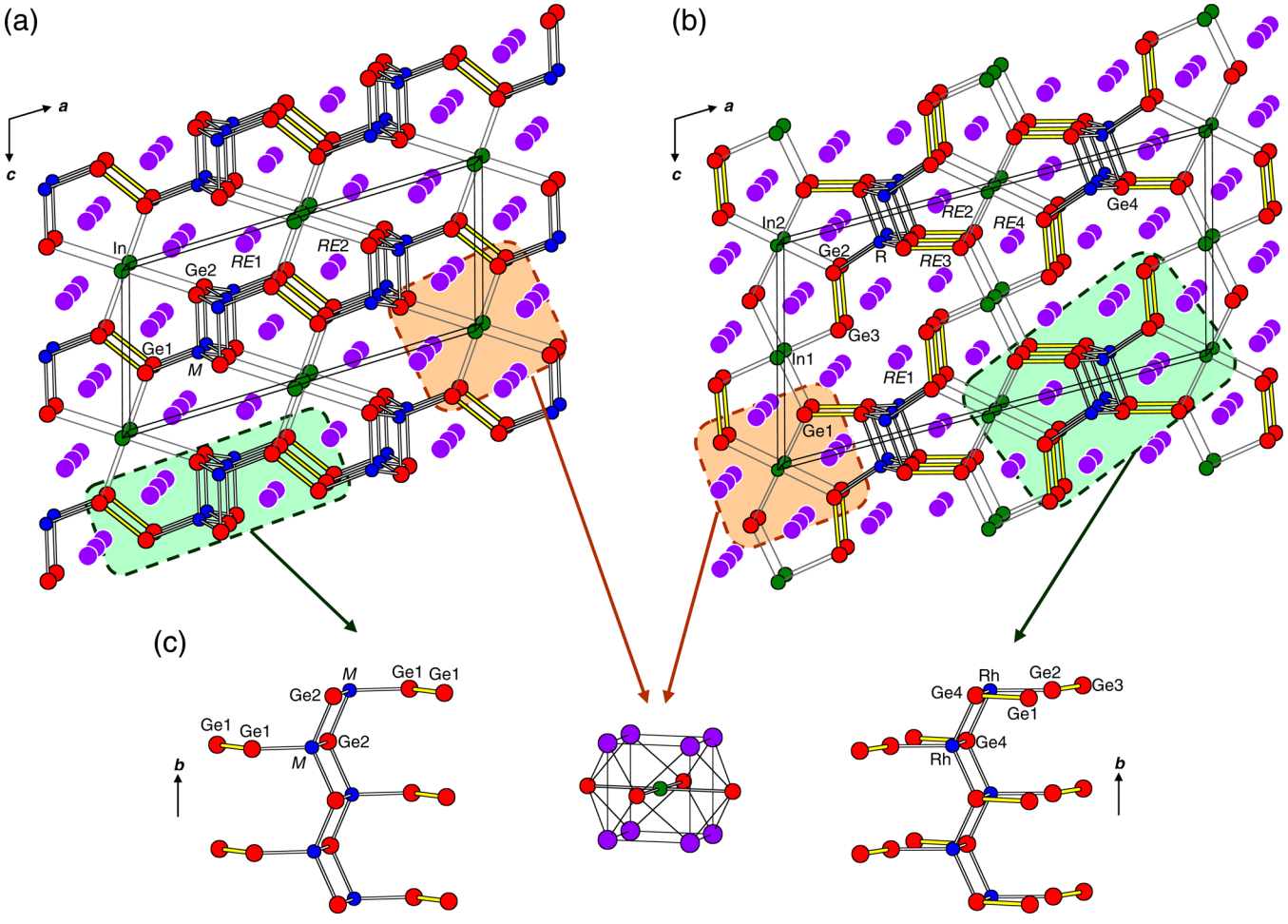

Figure 3. Structures of (a) $RE_4M_2InGe_4$ and (b) $RE_4RhInGe_4$ in terms of covalent frameworks built from (c) double chains of MGe_4 tetrahedra decorated with Ge_2 pairs, and In square planes embedded within tetragonal prisms of RE atoms. The large purple circles are RE atoms, the small blue circles are M atoms, the medium green circles are In atoms, and the medium red circles are Ge atoms.

DOI: 10.1021/ic502955h
Inorg. Chem. 2015, 54, 2780−2792

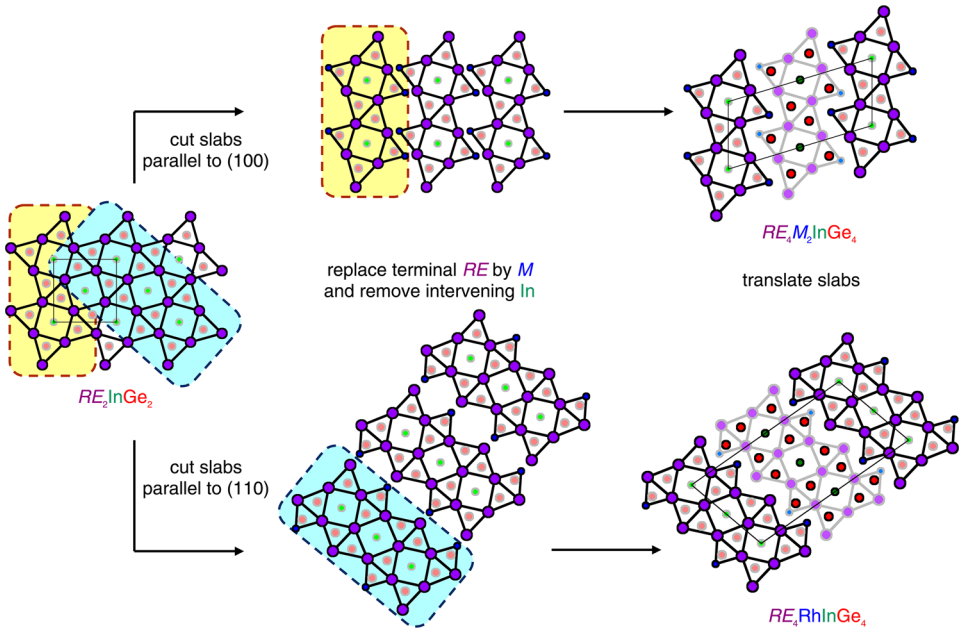

Figure 4. Derivation of $RE_4M_2InGe_4$ and $RE_4RhInGe_4$ from RE_2InGe_2, highlighting In-centered tetragonal prisms and Ge-centered trigonal prisms. Dark and light lines distinguish between atoms displaced by half the cell parameter along the viewing direction.

in other germanide structures, such as $RE_3M_2Ge_3$,[23] $Yb_2Zn_3Ge_3$,[24] $La_4Mg_7Ge_6$,[25] and $(Sr_{1-x}Ca_x)_5In_3Ge_6$.[26] The complete coordination environment around the In atoms includes eight RE atoms at the vertices of a tetragonal prism, augmented by four Ge atoms capping the waist. This 12-coordinate geometry is reduced in symmetry from an ideal cuboctahedron; while unusual, it is also encountered around the metalloid atoms in other structures (e.g., In in RE_2InGe_2;[5−8] Sn in $Yb_4Mn_2Sn_5$).[27]

Many intermetallic structures are often usefully described in terms of stackings of nets.[28] Although this approach may seem less appealing because it neglects consideration of bonding interactions, it provides other advantages in systematizing a large number of structures and drawing out the relationships between them. Previously we had shown that $RE_4M_2InGe_4$ can be derived from RE_2InGe_2.[13] The tetragonal (Mo_2FeB_2-type) structure of RE_2InGe_2 consists of a stacking of 3^2434 nets of RE atoms interleaved with $5^3 + 5^4$ (3:2) nets of In and Ge atoms.[8] (The Schläfli symbols indicate the types and numbers of polygons surrounding the nodes in a net of atoms.[28]) The In atoms lie over the squares, and the Ge atoms lie over the triangles of the RE nets, so that the structure of RE_2InGe_2 may be equally well-described in terms of In-centered tetragonal prisms and Ge-centered trigonal prisms. The structures of $RE_4M_2InGe_4$ and $RE_4RhInGe_4$ can now be generated through the identical procedure of excising slabs from RE_2InGe_2, separating these slabs and replacing the terminal RE atoms by M atoms, removing the intervening In atoms over cut squares, and translating these slabs parallel and perpendicular to the stacking direction so that the M atoms protruding from one slab rest in the notches of adjacent slabs to attain tetrahedral coordination by Ge atoms (Figure 4). The difference is that $RE_4M_2InGe_4$ is derived by cutting slabs parallel to (100), whereas $RE_4RhInGe_4$ is derived by cutting slabs parallel to (110). The derivation of complex structures through repetition by symmetry operations of parts of a simpler structure is, of course, a powerful systematizing principle in crystal chemistry.[29] The procedure of excising RE_2InGe_2-type slabs appears to have broader generality. For example, the structure of $(Eu_{1-x}Ca_x)_3In_2Ge_3$[30] can be derived by cutting slabs parallel to (100) that are thicker than those in $RE_4M_2InGe_4$ (Figure S5 in Supporting Information). It is also possible to imagine new target structures of hypothetical compounds that can be obtained by this procedure. This is not the only way to cut slabs, and other approaches are possible.

Analysis of bonding interactions suggests that the structure of $RE_4M_2InGe_4$ is dominated by strong covalent M−Ge and Ge−Ge bonds, which build up rigid $[M_2Ge_2]$ layers held together by weaker covalent bonds to In atoms and mostly ionic interactions to RE atoms. Inspection of interatomic distances (Table 4) confirms that M−Ge bonds change little upon substitution with smaller RE components (Fe−Ge, 2.431−2.500 Å; Co−Ge, 2.423−2.480 Å; Ru−Ge, 2.452−2.527 Å; Rh−Ge, 2.496−2.534) and are close to the sums of Pauling metallic radii (Fe−Ge, 2.41 Å; Co−Ge, 2.40 Å; Ru−Ge, 2.49 Å; Rh−Ge, 2.49 Å).[21] The significant distinction between the nearly constant Ge1−Ge1 distances within the Ge_2 dimers and the highly variable In−Ge distances within the $InGe_4$ squares is highlighted graphically (Figure 5). The Ge_2 dimers are only modestly affected by RE or M substitution, containing 2.5−2.6 Å distances that are close to the sum of metallic radii (2.48 Å) and similar to those found in many polygermanides. In contrast, the $InGe_4$ squares are actually highly distorted, with a pair of shorter In−Ge1 distances (2.9−3.1 Å) and a pair of longer In−Ge2 distances (3.2−3.4 Å). As M is substituted with Mn, Fe, Co, and Ru in this progression, the distances within these In−Ge pairs become more disparate such that the geometry around the In atoms could perhaps be better described as linear (CN2), as in the extreme case of $Ce_4Ru_2InGe_4$ (In−Ge1, 2.979 Å; In−Ge2, 3.451 Å). These distances are much longer than the sum of metallic radii (2.66 Å); relative to other situations of four-coordinate In atoms bonded to Ge atoms, they are longer than in those in tetrahedral geometry (e.g., 2.672−2.877 Å in $(Sr_{1-x}Ca_x)_5In_3Ge_6$)[26] but typical of those in square planar (e.g., 2.967−3.211 Å in $(Eu_{1-x}Ca_x)_4In_3Ge_4$)[30] or seesaw geometry (e.g., 2.823−2.942 Å in Ca_4InGe_4).[31]

DOI: 10.1021/ic502955h
Inorg. Chem. 2015, 54, 2780−2792

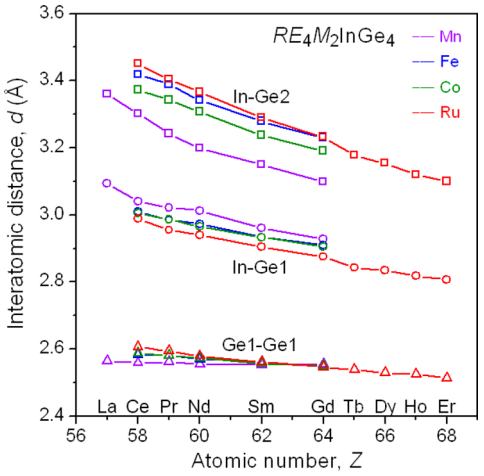

Figure 5. Plots of In−Ge1, In−Ge2, and Ge1−Ge1 distances in $RE_4M_2InGe_4$ (M = Mn, Fe, Co, Ru). Data for $RE_4Mn_2InGe_4$ are taken from ref 13.

It is tempting to account for the electronic structures of these quaternary germanides by applying a rudimentary Zintl formalism, as has been done for RE_2InGe_2.[8] To a good approximation, the electropositive RE atoms transfer their valence electrons entirely to form RE^{3+} cations. For RE_2InGe_2, the assumption of fully ionic character within the In−Ge bonds results in the oxidation state assignment of +3 for the In atoms within the square planes and −3 for the Ge atoms within the Ge_2 pairs, giving the formulation $(RE^{3+})_2(In^{3+})(Ge^{3-})_2(e^-)_3$, in which three excess electrons per formula unit enter the conduction band. Given the similar electronegativities of In (1.8) and Ge (2.0),[32] the more realistic assumption of fully covalent character within the In−Ge bonds results in the formal charge assignment of 1− for the four-bonded In atoms and 1− for the three-bonded Ge atoms, giving the alternative formulation $(RE^{3+})_2(In^{1-})(Ge^{1-})_2(e^-)_3$ with the same conclusion of an electron excess. For $RE_4M_2InGe_4$, the extension of these arguments leads to the formulations $(RE^{3+})_4(M^{2+})_2(In^{3+})(Ge^{3-})_2(Ge^{4-})_2(e^-)_5$ or $(RE^{3+})_4(M^{2+})_2(In^{1-})(Ge^{2-})_2(Ge^{3-})_2(e^-)_5$, if divalent M atoms are assumed. For $RE_4RhInGe_4$, these formulations are $(RE^{3+})_4(Rh^{3+})(In^{3+})(Ge^{3-})_4(e^-)_6$ or $(RE^{3+})_4(Rh^{3+})(In^{1-})(Ge^{1-})(Ge^{2-})_2(Ge^{3-})(e^-)_6$, if trivalent Rh atoms are assumed.

The electronic structure of $La_4Fe_2InGe_4$ (a hypothetical model based on the structure of $Ce_4Fe_2InGe_4$ but containing a nonmagnetic RE component) serves as a useful point of reference to examine the effects of substitution with a transition metal on progressing across a period (M = Mn, Fe, Co) or down a group (M = Fe, Ru). The Fermi level cuts through a substantial density of states (DOS) at the Fermi level, and there is no energy gap or deep pseudogap nearby that would be indicative of a Zintl phase (Figure 6a). Nevertheless, the formal charge assignments presented above are generally confirmed by the atomic projections, which show that the DOS is dominated by partly filled Fe, In, and Ge states up to the Fermi level and mostly empty La states above the Fermi level. The Fe 3d band extends from −4 to +2 eV; it is more than half-filled up to the Fermi level, consistent with a simple assignment of Fe^{2+}. The In 5s states are largely localized in a narrow band near −5 eV, and the In 5p states are dispersed widely from −4 eV upward. The distinction between Ge states belonging to the Ge1−Ge1 pair and the isolated Ge2 atoms can be clearly seen. The Ge1 states

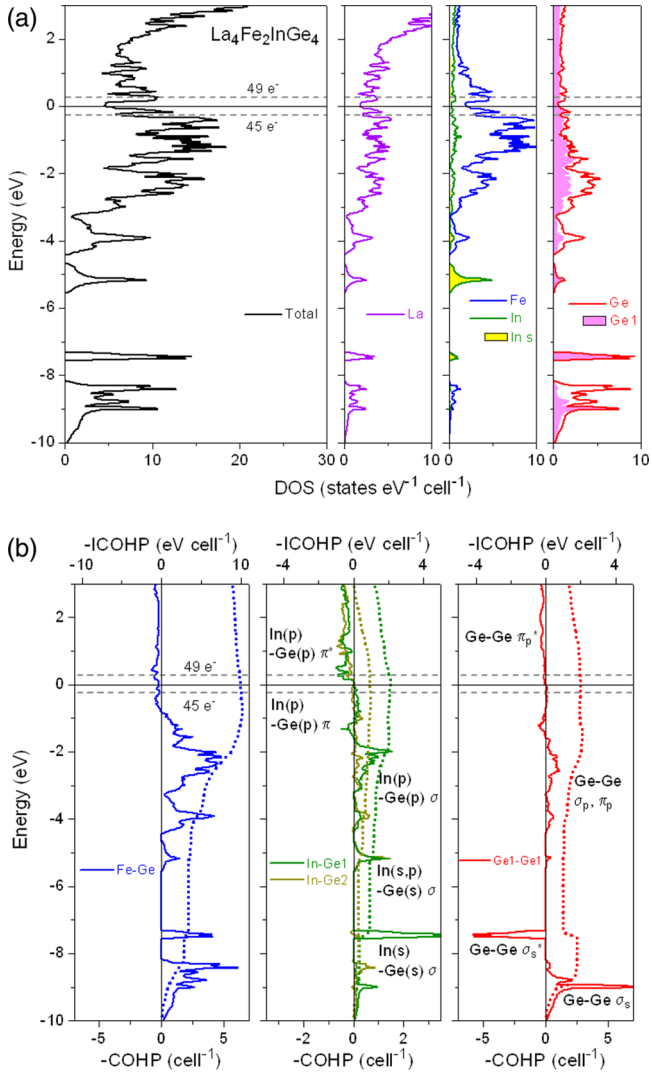

Figure 6. (a) Density of states (DOS) and its atomic projections for $La_4Fe_2InGe_4$. The Fermi level is at 0 eV for 47 e^-/f.u. The yellow shaded region in the third panel highlights the contribution of the In 5s states; the magenta shaded region in the last panel highlights the contribution of the Ge1 states involved in Ge1−Ge1 bonding. (b) Crystal orbital Hamilton population (COHP) curves for Fe−Ge, In−Ge, and Ge−Ge contacts.

follow the recognizable energy ordering for the molecular orbitals of a diatomic molecule, with the σ_s and σ_s* levels found near −9 and −7 eV, the σ_p and π_p levels from −5 to −1 eV, and the π_p* and σ_p* levels from −1 eV upward. In contrast, the Ge2 states do not show any splitting of the 4s states, being localized near −8.5 eV, while the 4p states are found in the manifold at higher energy (−4 eV upward).

A more detailed analysis of the bonding can be evaluated from the crystal orbital Hamilton population (COHP) curves (Figure 6b). In agreement with the description of the crystal structure in terms of rigid $[M_2Ge_2]$ layers, Fe−Ge and Ge−Ge contacts constitute the strongest type of bonding interactions. The Fe−Ge interactions are nearly optimized, with only weakly antibonding levels being present at the Fermi level; roughly, this situation corresponds to occupation of the *e* and some of the t_2 levels in an isolated $FeGe_4$ tetrahedral complex. The Ge−Ge interactions (originating from the Ge1−Ge1 pair) are net bonding, resulting from the occupation of the σ_s and σ_s* levels

DOI: 10.1021/ic502955h
Inorg. Chem. 2015, 54, 2780−2792

(which cancel each other out), the σ_p and π_p levels, and some of the π_p* levels. Given the relatively poor π-overlap of Ge 4p orbitals, it is not surprising that the π_p and π_p* levels represent weak (but nonneglible) interactions. In fact, the π_p* levels, which continue to extend well above the Fermi level (up to +10 eV), are barely occupied. In an isolated $(Ge^{3-})_2$ dimer, the π_p* levels would be completely filled, similar to the isoelectronic Br_2 molecule. It is worthwhile to understand why these π_p* levels have been depopulated within the solid. The reasons are related to the formation of the weak In−Ge bonds within the $InGe_4$ square planes.

In $RE_4M_2InGe_4$, the In−Ge distances are highly sensitive to substitution of the M component and, to a lesser extent, the RE component. All members of $RE_4M_2InGe_4$ exhibit distortion of this $InGe_4$ square plane, with the distance to the Ge1 atoms (belonging to the Ge1−Ge1 pair) being shorter than that to the isolated Ge2 atoms (Figure 7a). The stabilizing orbital

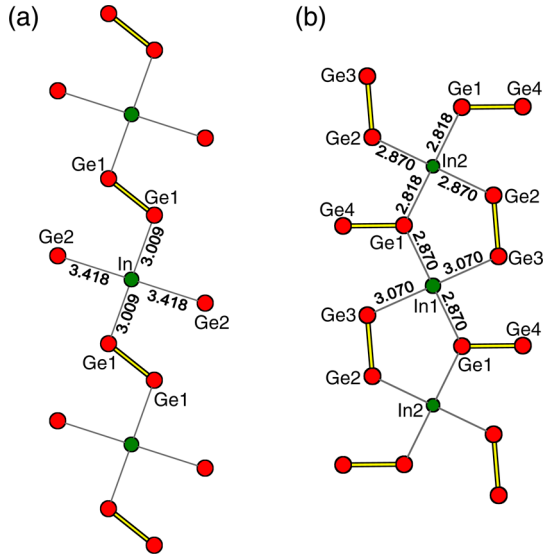

Figure 7. Connection of $InGe_4$ square planes in (a) $RE_4M_2InGe_4$ through Ge1−Ge1 pairs and Ge2 atoms and (b) $RE_4RhInGe_4$ through Ge1−Ge4 and Ge2−Ge3 pairs. The distances shown (in Å) refer to those found in the crystal structures of $Ce_4Fe_2InGe_4$ and $Tb_4RhInGe_4$, respectively.

interactions responsible for these In−Ge bonds can be traced to σ-overlap of In s with Ge s orbitals (−9 to −7 eV) and of In s/p with Ge s/p orbitals (−5 to −1 eV), as seen in the COHP curves. For example, the bonding peak in the In−Ge1 COHP curve at −2 eV can be attributed to Bloch functions in which the lobes of one set of the Ge1−Ge1 π_p orbitals (lying parallel to the $InGe_4$ plane) are directed toward the p-orbitals on In atom in a σ-fashion. At higher energies, weak π-overlap of In p with Ge p orbitals becomes operative; these interactions are nearly nonbonding just below the Fermi level (−2 to 0 eV) and become antibonding above. Similarly, the Ge−Ge interactions are nearly nonbonding in this region. Thus, $La_4Fe_2InGe_4$ attains a structure in which both In−Ge and Ge−Ge distances are adjusted to avoid the occupation of the antibonding levels, including the Ge−Ge π_p* levels mentioned above. To understand the origin of the distortion in the $InGe_4$ square plane, calculations were performed on models in which the In−Ge1 distances are contracted, while the In−Ge2 distances are expanded by the same increment of Δx relative to an idealized square plane with equal distances. The total energy decreases when these distortions are introduced and is minimized when Δx is 0.2 Å (Figure 8a), consistent with observations for the

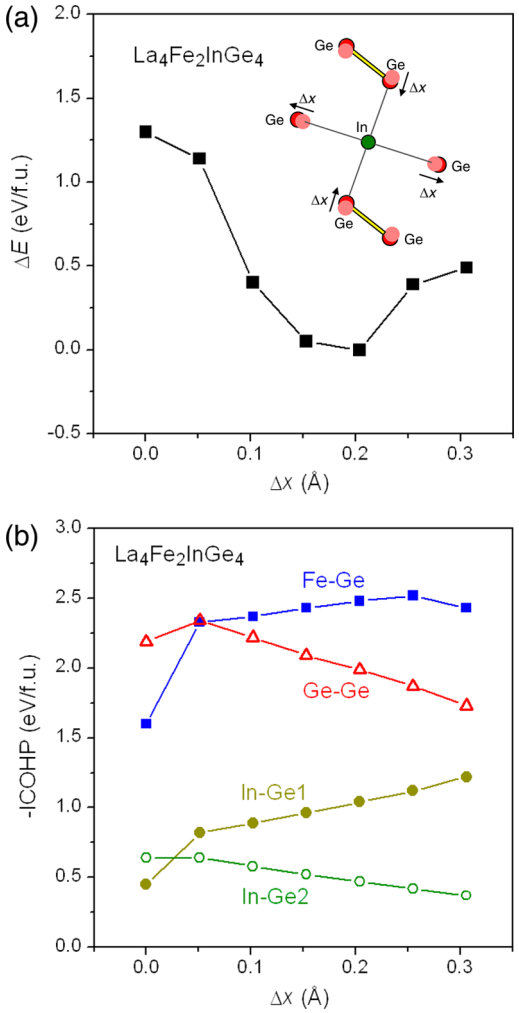

Figure 8. (a) Relative energy and (b) integrated COHP values (−ICOHP) for various contacts in $La_4Fe_2InGe_4$ models as the $InGe_4$ square plane is distorted from idealized equal In−Ge distances.

$RE_4Fe_2InGe_4$ series (Figure 5). A plot of the integrated COHP values (−ICOHP) for the different interactions is instructive (Figure 8b). The distortion of the $InGe_4$ square plane also affects the distances of the Ge1 and Ge2 atoms to the Fe atoms to which they are bonded. A key driving force is the need to satisfy good Fe−Ge contacts, which strengthen upon distortion of the $InGe_4$ square plane. Each Ge2 atom is bonded to three Fe atoms, whereas the Ge1 atom is only bonded to one Fe atom. Thus, it is favorable for the Ge2 atoms to sacrifice what little weak bonding they have to the In atoms to optimize their stronger bonding to the Fe atoms. Put another way, because the Ge2 atoms have already saturated their bonding capacity through their contacts with the Fe atoms, they have little incentive to bond to the In atoms.

From Figure 5, we recall that the general trend in the progression of M = Mn, Fe, Co in $RE_4M_2InGe_4$ is that the distortion of the $InGe_4$ square plane tends to become more pronounced. If a rigid band approximation is applied, starting from the band structure of $La_4Fe_2InGe_4$, increasing the electron count would lead to greater occupation of antibonding levels for all types of bonds (Figure 6b). At the same time, the d-band

DOI: 10.1021/ic502955h
Inorg. Chem. 2015, 54, 2780−2792

of the transition metal would drop down in energy and become more filled, as confirmed in the actual DOS curves for $La_4M_2InGe_4$ (M = Mn, Fe, Co), compared in Figure 9. In

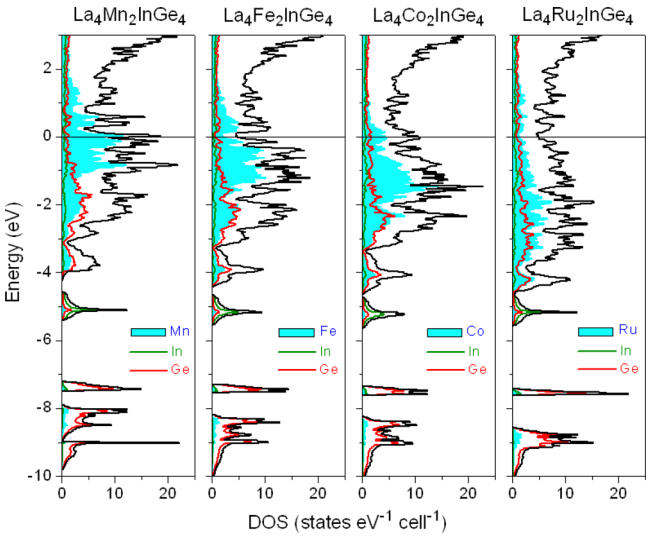

Figure 9. DOS and atomic projections for $La_4M_2InGe_4$ (M = Mn, Fe, Co, Ru).

reality, what happens is that the M−Ge interactions are always optimized, because they are the most important. To counteract the population of antibonding levels if the electron count is increased, the effect of distorting the $InGe_4$ square plane further is to stabilize In−Ge bonding levels and raise In−Ge antibonding ones, such that the states near the Fermi level are always close to being nonbonding. Note, for example, that the In 5s peak is located at −5.0 eV in $La_4Mn_2InGe_4$ and is lowered slightly to −5.2 eV in $La_4Co_2InGe_4$. Comparing $La_4Fe_2InGe_4$ and $La_4Ru_2InGe_4$ illustrates the replacement of the transition-metal component going down a group. The d-band in $La_4Ru_2InGe_4$ is more disperse than in $La_4Fe_2InGe_4$; the net effect is equivalent to a greater filling of the d-band, which would also lead to more distortion of the $InGe_4$ square plane.

With the insight gained by analyzing the electronic structure of the $La_4M_2InGe_4$ models above, we can proceed to examine $Y_4RhInGe_4$ (as a model for $Tb_4RhInGe_4$ but containing a nonmagnetic RE component) and see if the same conclusions hold. The DOS and COHP curves (Figure 10) show the same general features found for $La_4M_2InGe_4$, except that there are now two types of Ge_2 pairs, reflected by the appearance of two sets of σ_s and σ_s* levels (located near −9.5 and −7.9 eV for Ge2−Ge3, or −9.9 and −8.2 eV for Ge1−Ge4). The $InGe_4$ square planes are linked via these Ge_2 pairs acting as bridging ligands between the In1 and In2 atoms to form a chain (Figure 7b). Both atoms in the Ge2−Ge3 pairs, which are aligned parallel to the chain, are bonded to the In atom, but only the Ge1 atom in the Ge1−Ge4 pairs, which are oriented perpendicularly to the chain, is bonded to the In atom. Among the Ge atoms bonded directly to the In atom, only Ge2 is also bonded to one Rh atom. In contrast to $La_4M_2InGe_4$, the orbitals on all these Ge atoms are little or not used for Rh−Ge bonding and instead can interact strongly with the In atoms. Thus, the In−Ge distances are much less disparate within the $InGe_4$ square planes.

Inspection of −ICOHP values in $La_4M_2InGe_4$ and $Y_4RhInGe_4$ structures confirms that the strongest types of

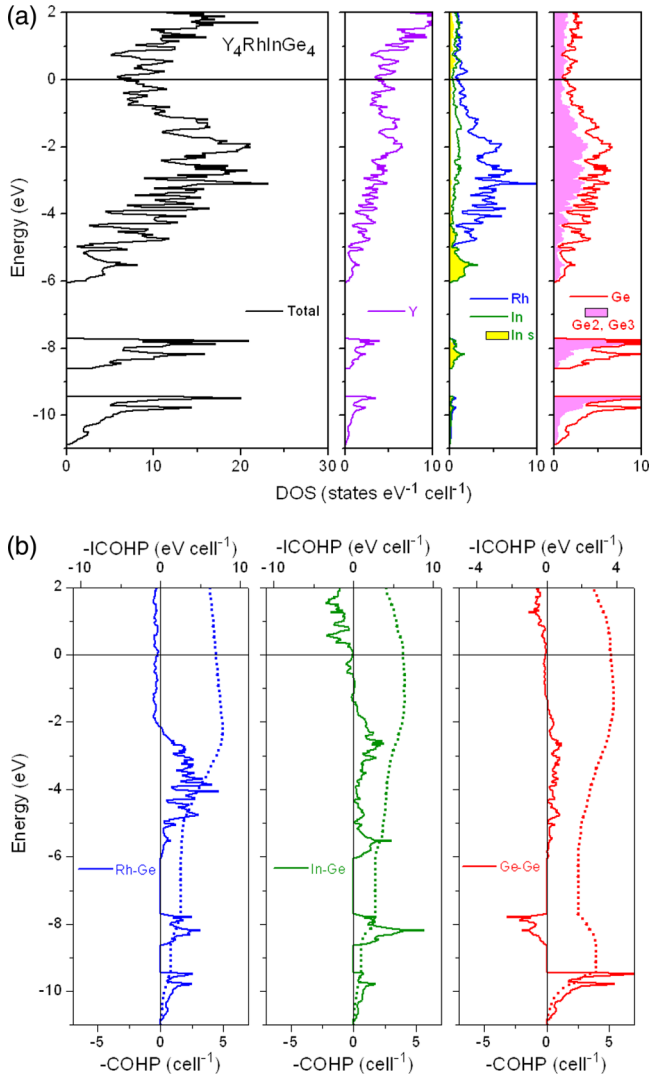

Figure 10. (a) DOS and atomic projections for $Y_4RhInGe_4$. In the last panel, the magenta shaded region highlights the contribution of states involved in Ge2−Ge3 bonding; what remains belongs to states involved in Ge1−Ge4 bonding. (b) COHP curves for Rh−Ge, In−Ge, and Ge−Ge bonding.

covalent bonds are M−Ge, followed by Ge−Ge and then In−Ge interactions (Table 5). However, when multiplied by the number of contacts present in the structure, In−Ge interactions contribute a greater proportion than Ge−Ge interactions to the bonding stability per unit cell. Moreover, in $Y_4RhInGe_4$, there are more $InGe_4$ squares and Ge_2 pairs than there are in $La_4M_2InGe_4$; correspondingly, In−Ge and Ge−Ge interactions contribute significantly more to the bonding stability relative to $La_4M_2InGe_4$. Within the distorted $InGe_4$ square plane in $La_4M_2InGe_4$, the shorter In−Ge contacts (3.0 A; −ICOHP of 1.0 eV/bond) are nearly twice as strong as the longer In−Ge contacts (3.3−3.4 Å; −ICOHP of 0.5−0.6 eV/bond). Interestingly, within the much less distorted $InGe_4$ square plane in $Y_4RhInGe_4$, this difference in −ICOHP values is still retained even though the two sets of In−Ge contacts differ by only 0.1−0.2 Å. In fact, even though they have the same length of 2.870 Å, the shorter set of contacts within the In1-centered square is twice as strong (In1−Ge1; −ICOHP of 1.12 eV/bond) than the longer set of contacts within the In2-centered square (In2−Ge2; −ICOHP of 0.58 eV/bond). As noted

DOI: 10.1021/ic502955h
Inorg. Chem. 2015, 54, 2780−2792

Table 5. Integrated Crystal Orbital Hamilton Populations for $La_4M_2InGe_4$ (M = Mn, Fe, Co, Ru) and $Y_4RhInGe_4$ Models

	distances (Å)	−ICOH P (eV/bond)	−ICOHP (eV/cell)	contribution (%)
$La_4Mn_2InGe_4$				
Mn−Ge	2.589 (×2)	2.32 (×2)	9.04	63.0
	2.615	2.34		
	2.626	2.05		
In−Ge	3.040 (×2)	0.98 (×2)	3.18	22.2
	3.302 (×2)	0.61 (×2)		
Ge−Ge	2.558	2.12	2.12	14.8
$La_4Fe_2InGe_4$				
Fe−Ge	2.461 (×2)	2.58 (×2)	9.91	66.5
	2.490	2.48		
	2.500	2.27		
In−Ge	3.009 (×2)	1.04 (×2)	3.02	20.2
	3.418 (×2)	0.47 (×2)		
Ge−Ge	2.583	1.99	1.99	13.3
$La_4Co_2InGe_4$				
Co−Ge	2.444 (×2)	2.46 (×2)	9.46	64.9
	2.480	2.33		
	2.473	2.20		
In−Ge	3.006 (×2)	1.05 (×2)	3.14	21.6
	3.372 (×2)	0.52 (×2)		
Ge−Ge	2.588	1.97	1.97	13.5
$La_4Ru_2InGe_4$				
Ru−Ge	2.479 (×2)	2.77 (×2)	10.61	68.4
	2.527	2.55		
	2.504	2.52		
In−Ge	2.979 (×2)	1.09 (×2)	3.02	19.5
	3.451 (×2)	0.42 (×2)		
Ge−Ge	2.606	1.87	1.87	12.1
$Y_4RhInGe_4$				
Rh−Ge	2.470 (×2)	1.69 (×2)	6.92	41.5
	2.542	1.59		
	2.552	1.95		
In−Ge	2.870 (×2)	1.12 (×2)	6.14	36.8
	3.070 (×2)	0.37 (×2)		
	2.818 (×2)	1.00 (×2)		
	2.870 (×2)	0.58 (×2)		
Ge−Ge	2.596	1.95	3.63	21.7
	2.619	1.68		

above, the Ge2 atom also participates in orbital interactions to the Rh atom; the weakness of the In2−Ge2 bond despite its "short" distance reflects a matrix effect rather than robust bonding.

Relatively little is known about the magnetic properties of $RE_4M_2InGe_4$ compounds; only a few members of the Ni-containing series have been previously analyzed (RE = Dy, Ho, Er, Tm), and these were found to undergo antiferromagnetic ordering at low temperatures.[10] To examine the effect of substitution of the M component, magnetic susceptibility measurements were made for several Sm-containing members $Sm_4M_2InGe_4$ (M = Fe, Co, Ru, Rh), which were also the only samples that could be prepared free of other phases (Figure 11). The magnetic susceptibility curves obtained under zero-field-cooled and field-cooled conditions are superimposable. Typical of many Sm-containing intermetallic compounds, the magnetic susceptibility is low and cannot be fit to the Curie−Weiss law (as indicated by strong curvature in the inverse susceptibility curves, not shown); the effective magnetic

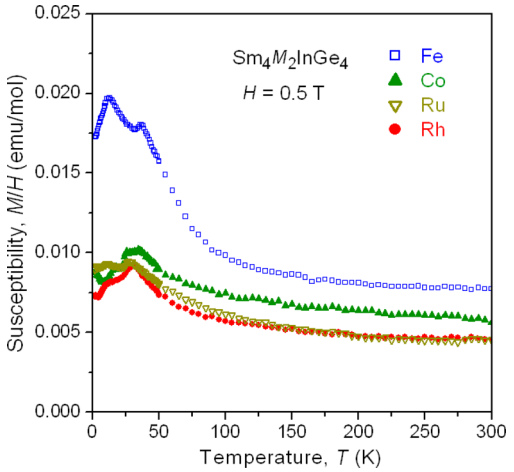

Figure 11. Magnetic susceptibility for $Sm_4M_2InGe_4$ (M = Fe, Co, Ru, Rh).

moment can deviate significantly from the expected value for a free Sm^{3+} ion because of the occupation of low-lying excited states above the ground state (J = 5/2) multiplet and the influence of crystal field effects. Attempts to fit the magnetic susceptibility to the modified Curie−Weiss law yielded effective magnetic moments that are higher than expected (e.g., 1.0(1) μ_B for $Sm_4Fe_2InGe_4$, compared to 0.85 μ_B for a free Sm^{3+} ion), indicating that population of excited states is important. There are two peaks in the magnetic susceptibility curves near 30 and 10 K for M = Fe, Ru, and Rh, and possibly more complicated transitions for M = Co. Similar peaks are observed in the low-temperature behavior for $Dy_4Ni_2InGe_4$ (30 and 11 K) and $Ho_4Ni_2InGe_4$ (10 and 4 K), for which spin reorientation processes are the most likely origin.[10] The magnetic behavior of all these compounds is dominated by the RE component but little influenced by the M component, implying strong delocalization of the d-electrons of the transition-metal atoms. This is consistent with the relatively low contribution of d-states to the DOS at the Fermi level in the band structures for $La_4M_2InGe_4$ (M = Fe, Co, Ru) seen earlier (Figure 9). RKKY interactions in which the magnetic moments of the RE atoms are coupled through the mediation of conduction electrons are the likely mechanism for the magnetic behavior. In contrast, the contribution of d-states to the DOS at the Fermi level for $La_4Mn_2InGe_4$ is markedly greater, so spin polarization of the d-band can potentially take place. It would thus be interesting to examine the magnetic properties of the Mn-containing series in future investigations.

CONCLUSIONS

A large number of quaternary germanides $RE_4M_2InGe_4$ can be prepared through arc-melting and annealing reactions at 800 °C, without requiring the use of an In flux, indicating that these are thermodynamically stable phases. Their diversity has been considerably expanded through the substitution of the M component, which can range from the mid-to-late transition metals (M = Mn, Fe, Co, Ni, Ru, Rh, Ir). A related series $RE_4RhInGe_4$ was identified in the course of this investigation. The monoclinic structures of both $RE_4M_2InGe_4$ and $RE_4RhInGe_4$ can be elegantly derived from the more symmetrical tetragonal RE_2InGe_2 structure by excision of slabs in different directions and translating these slabs. New target structures may be envisioned from this approach by

DOI: 10.1021/ic502955h
Inorg. Chem. 2015, 54, 2780−2792

cutting slabs in other directions. Size effects contribute to the range of RE substitution possible in a given $RE_4M_2InGe_4$ series, through appropriate matching of RE and M radii, and narrowly restrict the limits of formation of $RE_4RhInGe_4$. Electronic effects account for trends seen in the characteristic $InGe_4$ square planes in $RE_4M_2InGe_4$, which undergo distortions to balance the competition between the strong M−Ge bonds within MGe_4 tetrahedra and the weaker but more responsive In−Ge bonds within the square planes. The Ge−Ge bonds within the Ge_2 dimers are little affected by substitutions in M because their interactions are largely nonbonding near the Fermi level, a consequence of poor π-overlap between p orbitals on the Ge atoms. To probe the interplay between M−Ge, In−Ge, and Ge−Ge bonding, it will be interesting to attempt replacement of the In atoms by other atoms (perhaps Cd) in the square planar sites or Ge atoms by other p-block elements (perhaps Si) that may be prone to form dimers. The physical properties of these series deserve further investigation.

■ ASSOCIATED CONTENT

Supporting Information

X-ray crystallographic files in CIF format, full crystallographic details, powder XRD patterns, EDX spectra, and additional structural figures. This material is available free of charge via the Internet at http://pubs.acs.org. Additional CIF files may be obtained from Fachinformationszentrum Karlsruhe, Abt. PROKA, 76344 Eggenstein-Leopoldshafen, Germany (No. CSD-428855 to 428875).

■ AUTHOR INFORMATION

Corresponding Author

*E-mail: arthur.mar@ualberta.ca.

Notes

The authors declare no competing financial interest.

■ ACKNOWLEDGMENTS

This work was supported by the Natural Sciences and Engineering Research Council of Canada.

■ REFERENCES

(1) Salamakha, P. S.; Sologub, O. L.; Bodak, O. I. In *Handbook on the Physics and Chemistry of Rare Earths;* Gschneidner, K. A., Jr., Eyring, L., Eds.; Elsevier: Amsterdam, 1999; Vol. *27*, pp 1−223.
(2) Bie, H.; Zelinska, O. Ya.; Tkachuk, A. V.; Mar, A. *Chem. Mater.* **2007**, *19*, 4613−4620.
(3) Mudryk, Y.; Pecharsky, V. K.; Gschneidner, K. A., Jr. *Z. Anorg. Allg. Chem.* **2011**, *637*, 1948−1956.
(4) Sung, N. H.; Roh, C. J.; Kim, K. S.; Cho, B. K. *Phys. Rev. B* **2012**, *86*, 224507−1−224507−6.
(5) Zaremba, V. I.; Stępień-Damm, A.; Nichiporuk, G. P.; Tyvanchuk, Yu. B.; Kalychak, Ya. M. *Kristallografiya* **1998**, *43*, 13−16.
(6) Zaremba, V. I.; Kaczorowski, D.; Nychyporuk, G. P.; Rodewald, U. Ch.; Pöttgen, R. *Solid State Sci.* **2004**, *6*, 1301−1306.
(7) Zaremba, V. I.; Johrendt, D.; Rodewald, U. Ch.; Nychyporuk, G. P.; Pöttgen, R. *Solid State Sci.* **2005**, *7*, 998−1002.
(8) Tobash, P. H.; Lins, D.; Bobev, S.; Lima, A.; Hundley, M. F.; Thompson, J. D.; Sarrao, J. L. *Chem. Mater.* **2005**, *17*, 5567−5573.
(9) Rieger, W.; Nowotny, H.; Benesovsky, F. *Monatsh. Chem.* **1964**, *95*, 1502−1503.
(10) Salvador, J. R.; Kanatzidis, M. G. *Inorg. Chem.* **2006**, *45*, 7091−7099.
(11) Chondroudi, M.; Balasubramanian, M.; Welp, U.; Kwok, W.-K.; Kanatzidis, M. G. *Chem. Mater.* **2007**, *19*, 4769−4775.
(12) Chondroudi, M.; Peter, S. C.; Malliakas, C. D.; Balasubramanian, M.; Li, Q. A.; Kanatzidis, M. G. *Inorg. Chem.* **2011**, *50*, 1184−1193.
(13) Oliynyk, A. O.; Stoyko, S. S.; Mar, A. *Inorg. Chem.* **2013**, *52*, 8264−8271.
(14) Chumalo, N.; Nychyporuk, G. P.; Pavlyuk, V. V.; Pöttgen, R.; Kaczorowski, D.; Zaremba, V. I. *J. Solid State Chem.* **2010**, *183*, 2963−2967.
(15) Dominyuk, N.; Zaremba, V. I.; Pöttgen, R. *Z. Naturforsch., B.: Chem. Sci.* **2011**, *66*, 433−436.
(16) Akselrud, L. G.; Zavalii, P. Yu.; Grin, Yu. N.; Pecharski, V. K.; Baumgartner, B.; Wölfel, E. *Mater. Sci. Forum* **1993**, *133−136*, 335−342.
(17) Sheldrick, G. M. *SHELXTL,* version 6.12; Bruker AXS Inc.: Madison, WI, 2001.
(18) Gelato, L. M.; Parthé, E. *J. Appl. Crystallogr.* **1987**, *20*, 139−143.
(19) Oliynyk, A. O.; Djama-Kayad, K.; Mar, A. *J. Alloys Compd.* **2015**, *622*, 837−841.
(20) Tank, R.; Jepsen, O.; Burkhardt, A.; Andersen, O. K. *TB-LMTO-ASA Program,* version 4.7; Max Planck Institut für Festkörperforschung: Stuttgart, Germany, 1998.
(21) Pauling, L. *The Nature of the Chemical Bond,* 3rd ed.; Cornell University Press: Ithaca, NY, 1960.
(22) Salamakha, P. S. In *Handbook on the Physics and Chemistry of Rare Earths;* Gschneidner, K. A., Jr., Eyring, L., Eds.; Elsevier: Amsterdam, 1999; Vol. *27*, pp 223−338.
(23) Oliynyk, A. O.; Stoyko, S. S.; Mar, A. *J. Solid State Chem.* **2013**, *202*, 241−249.
(24) Grytsiv, A.; Kaczorowski, D.; Rogl, P.; Tran, V.; Godart, C.; Gofryk, K.; Giester, G. *J. Phys.: Condens. Matter* **2005**, *17*, 385−397.
(25) Solokha, P.; De Negri, S.; Skrobanska, M.; Saccone, A.; Pavlyuk, V.; Proserpio, D. M. *Inorg. Chem.* **2012**, *51*, 207−214.
(26) You, T.-S.; Bobev, S. *J. Solid State Chem.* **2010**, *183*, 1258−1265.
(27) Lei, X.-W.; Zhong, G.-H.; Li, M.-J.; Mao, J.-G. *J. Solid State Chem.* **2008**, *181*, 2448−2455.
(28) Pearson, W. B. *The Crystal Chemistry and Physics of Metals and Alloys;* Wiley: New York, 1972.
(29) Hyde, B. G.; Andersson, S. *Inorganic Crystal Structures;* Wiley: New York, 1989.
(30) You, T.-S.; Tobash, P. H.; Bobev, S. *Inorg. Chem.* **2010**, *49*, 1773−1783.
(31) You, T.-S.; Jung, Y.; Bobev, S. *Dalton Trans.* **2012**, *41*, 12446−12451.
(32) Allred, A. L. *J. Inorg. Nucl. Chem.* **1961**, *17*, 215−221.

DOI: 10.1021/ic502955h
Inorg. Chem. 2015, 54, 2780−2792